HYDROLOGIC MODEL FRAMEWORK FOR WATER RESOURCES PLANNING IN THE SANTA-CRUZ RIVER, SOUTHERN ARIZONA

Eylon Shamir[1*], David M. Meko[2], Nicholas, E. Graham[1,3], and Konstantine P. Georgakakos[1,3]

[(1)] Hydrologic Research Center, 12780 High Bluff Drive, Suite 250, San Diego, CA 92130; Tel: 1-858-794-2726; Fax: 1-858-792-2519; E-mail: EShamir@hrc-lab.org

[(2)] Laboratory of Tree-Ring Research, University of Arizona, Tucson, AZ 85721

[(3)] Scripps Institution of Oceanography, UCSD, La Jolla, CA 92093-0224

* Corresponding Author

Submitted: April 3, 2006

Reviewed: December 8, 2006

Revised and resubmitted: January 3, 2007

ABSTRACT

The authors develop a model framework that includes a set of hydrologic modules as a water resources management and planning tool for the upper Santa Cruz River near the Mexican border, Southern Arizona. The modules consist of: 1) stochastic generation of hourly precipitation scenarios that maintain the characteristics and variability of a 45-year hourly precipitation record from a nearby raingauge; 2) conceptual transformation of generated precipitation into daily streamflow using varied infiltration rates and estimates of the basin antecedent moisture conditions; and 3) surface-groundwater interaction for four downstream microbasins that accounts for alluvial groundwater recharge, and ET and pumping losses. To maintain the large inter-annual variability of streamflow as prevails in Southern Arizona, the model framework is constructed to produce three types of seasonal winter and summer categories of streamflow (i.e., wet, medium or dry). Long term (i.e., 100 years) realizations (ensembles) are generated by the above described model framework that reflects two different regimes of inter annual variability. The first regime is that of the historic streamflow gauge record. The second regime is that of the tree ring reconstructed precipitation which was derived for the study location. Generated flow ensembles for these two regimes are used to evaluate the risk that the regional four groundwater microbasins decline below a preset storage threshold under different operational water utilization scenarios.

(KEY TERMS: water management; ephemeral streams; stochastic hydrology; rainfall data simulation; groundwater modeling; Dendrochronology; alluvial recharge)

INTRODUCTION

This study is concerned with the region of the upper Santa Cruz River in arid southern Arizona near the international border between U.S and Mexico. This region which depends exclusively on groundwater reservoirs has experienced population growth rate of about 8% a year in the last 10 years, and concurrent increase in potable water demand (Arizona Department of Water Resources, 1999). Water supply in this region relies on groundwater exploitation of relatively shallow aquifer formations. The intermittent flow events on the ephemeral Santa Cruz River are the major source of groundwater recharge through the highly conductive alluvium bed. Sustainable development in this region is a critical concern because of increasing trends of regional economic and population growth under a limited water supply, which is potentially affected by climate variability (e.g., Gleick and Adams, 2000; Hanson *et al.,* 2005). In this context, sustainable development is defined by the World Commission on Environment and Development (1987) to be "the development that meets the needs of the present without compromising the ability of the future generation to meet their own needs." In practical management of regional groundwater reservoirs, sustainable development is achieved by maintaining a *safe yield*. The term safe yield has various definitions but in general it is the attainment and maintenance of a long-term balance between groundwater withdrawals and recharge (Alley, 2001).

To promote sustainable development, the State of Arizona established the Assured Water Supply Program according to which new residential developments and water suppliers must demonstrate that their existing, committed, and reasonably foreseeable future water demands can be met using renewable water supplies over a 100-year period (http://www.azwater.gov/WaterManagement_2005/Content/Forms/AWSBrochure.pdf). The goal of the Santa Cruz Active Management Area (SCAMA) in arid southern Arizona is to conjunctively manage all water resources in the AMA and to assure reliable water supply for current and future uses, protecting aquatic and riparian habitat while sustaining a healthy economy. The management goal of the SCAMA is to maintain a safe-yield condition and prevent local water tables from experiencing long term declines (Arizona Department of Water Resources, 1999).

A simple analysis of the Santa Cruz River flow record makes apparent the large variability and complexity in streamflow patterns. For instance, the average observed water-year (October 1 – September 30) daily mean flow in the river ranged from minimum of 1 to a maximum of 123 ft^3s^{-1} (0.03 - 3.5 m^3s^{-1}) with an average of 26 ft^3s^{-1} (0.7 m^3s^{-1}). The water-year coefficient of variation was about 2, 4 and 8 for the minimum average and maximum daily flow, respectively. In addition, the average percentage of the time that daily flow was observed during the water year is 50%, and this ranged from a minimum of 3% to a maximum of about 90%. If regional planning goals enforce long-term balance between the annual aquifer exploitation with the annual net groundwater recharge from streamflow, it becomes clear that the large variability in flow magnitude and the flow intermittence must be considered in any projections used for long term water resources planning.

In this study we present a modeling framework that was developed to generate information for the long term planning of the utilization of the groundwater resources in the aquifers that underline the alluvium bed of the upper Santa Cruz River. The study formulates and applies a hydrologic model that reproduces the within-year and the year-to-year flow variability. The hydrologic model is presented in a companion paper by Shamir *et al*., (2007). For the description of the variability from year to year, in addition to the historical streamflow record, we utilized a paleoclimatic record of precipitation estimates that was reconstructed from tree ring records for the study area.

SETTING

Study Site

The Santa Cruz River is an ephemeral tributary in Southern Arizona that drains into Gila River, which is a branch of the Colorado River (Figure 1). The drainage area of concern in this study is defined by the USGS Nogales gauge (USGS # 09480500), which is located about 10 km east of the city of Nogales, Arizona. This drainage area is about 1,400 km^2, of which approximately 1,150 km^2 are in Mexico. From its headwaters in the San Rafael Valley in Southern Arizona, the river flows southward into Mexico and then bends northwards towards Arizona crossing again the international border. The river

length in Mexico is about 60 km with some sections that maintain perennial flow. The drainage area is sparsely populated and the land cover consists of heavily grazed dessert scrub with broad leaf forest in the higher elevations. The elevation ranges from 1,150 m at the gauge site to 2,160 m above sea level on the mountain tops. About 85% of the basin area is below 1,600 m.

Downstream of the Nogales gauge there is a series of four relatively small alluvial groundwater microbasins surrounded by a very low-permeability formation (Nogales Formation). The microbasins are separated from each other by outcrops of the Nogales Formation and/or shallow bedrock. These constrictions are generally referred to as narrows and limit the hydraulic connection between the microbasins (Halpenny and Halpenny, 1991). The microbasins listed from south to north are Buena Vista, Kino Springs, Highway 82, and Guevavi. The microbasins are comprised of younger alluvium which is highly productive with transmissivity values ranging from 400 to 2,800 $m^3 d^{-1}$.

The major natural replenishment of the downstream groundwater microbasins that accounts for about 90% of the annual recharge is formed by the intermittent flow events in the Santa-Cruz River. Other possible sources of recharge for these microbasins are under flow from Mexico, mountain front recharge, lateral flow from the adjacent aquifer, incidental recharge from agriculture or diffused recharge from precipitation (Erwin, 2007). The thickness of the younger alluvium ranges from 10 to 40 meters and the depth to water is generally less than 3 meters below the land surface. However, during drought periods the depth to water can reach down to 15 meters (Erwin, 2007). Existing and predicted urban development downstream of the Nogales gauge raises concern regarding the sustainable management of the ground water reservoirs (ADWR, 1999). Additional description of the dimensions and physical characteristics of each microbasin is provided in Table 2.

Data

In this study we used a complete mean daily flow record from 7/1/1935 to 9/30/2003 for the Nogales gauge. Hourly precipitation data is compiled and published by the National Climatic Data Center and was acquired from EarthInfo, Inc. The precipitation record consists of cumulative hourly data for the period between 7/1/1948 to

12/31/1992. This time series was compiled from two gauges. The first (W110:55, N31:21) has a record from 7/1/1948 to 12/31/1983, while the second which is located at the Nogales International Wastewater Treatment Plant (W110:57, N31:25), has a record from 1/8/1983-12/31/1992.

The areal distribution of the winter precipitation over the basins was evaluated in Shamir *et al*., (2007) with retrospective high-resolution atmospheric mesoscale model simulations of six representative winter storms. The results from the model indicate that the precipitation rates were comparable to that simulated for the precipitation gauge location for most of the basin area that contributes to the Nogales streamflow gauge.

DATA ANALYSIS

Season definition

The region has two major wet seasons: the summer (July-September), and winter (November-March). The summer storms are mainly driven by isolated convective cells, while the winter storms are originated from large scale low pressure frontal systems (Sheppard *et al*., 1999). Summer precipitation is primarily of monsoonal origin with some contribution from remnants of Pacific tropical storms. Winter precipitation is almost entirely from frontal storms approaching from the west and southwest. These two types of storm dynamics yield different storm characteristics with different characteristics of streamflow hydrographs. The mean annual precipitation at the Nogales gauge for 1914-2000 was 422 mm, with average 59% and 29% observed in summer and winter, respectively.

The spring (April-June) is usually dry and the fall (October) is dry with occasionally intense rainfall that generates high flow. The rare occurrences of precipitation during the dry spring season are both from winter-type systems and early monsoon episodes. The month of October is relatively dry with some contribution from all three sources and includes instances of heavy rainfall associated with tropical storm activity.

Climate indices

To better understand and quantify any influences of climatic variability so that we identify such influences to incorporate in the models, we performed a diagnostic study of the relationship of precipitation to climatic indices. A composite seasonal precipitation dataset for the Nogales area was prepared covering 1914-2000. The NINO3 index, which is the areal average sea surface temperature (SST) anomaly over the region 150-90˚W, 5˚S-5˚N (Kaplan *et al*., 1997), was used to characterize El Niño activity. Decadal-scale Pacific climate variability was characterized by the Pacific Decadal Oscillation (PDO) index (Mantua *et al*., 1997). This index characterizes sea surface temperature fluctuations in the central North Pacific (cool SSTs give high values of the PDO index), and is an indicator of the strength of the winter westerlies and storm track activity in that region. High values of the PDO are associated with generally higher precipitation across the southwestern US in the modern record.

Correlations between seasonal Nogales precipitation and the NINO3 and PDO indices are shown in Table 1. It can be seen that when the data are treated on a season-by-season basis, only the El Niño signal has substantial relationship with Nogales precipitation, and this only for winter. The relationship between El Niño and Nogales precipitation is typical of such relationships in the western US (e.g., Redmond and Koch, 1991) and implies increasing annual precipitation with increasing NINO3 SST. The lack of a strong relationship between El Niño variability and regional precipitation in other seasons is in agreement with earlier analyses (e.g., Webb and Bettencourt, 1990; Pool 2005).

The well known relationship between Southwest rainfall and the PDO (e.g., Cayan *et al.,* 1998) becomes apparent when the precipitation records are smoothed, though there is little to distinguish effects apparently related to the PDO or with the smoothed El Niño signal (El Niño years are also associated with storminess and cool North Pacific SSTs). Therefore, it is not possible to clearly distinguish independent effects from the PDO or El Niño (Zhang *et al.,* 1997), especially with a record this short in comparison to the time scales of interest (multi-decadal). The effects of El Niño on the Nogales winter precipitation record were removed using linear regression, and residuals from that analysis were then compared with the PDO record. The results showed that the

PDO explained almost none of the residual record, reinforcing the difficulty in assessing clearly independent effects of decadal variability in El Niño and the PDO.

Also shown in Table 1 are correlations between the precipitation average for Arizona Climate Division 7 (most of southernmost Arizona) and Nogales precipitation, again for the seasons defined earlier. These correlations emphasize how changes in the spatial scales of precipitation systems alter correlations between point measurements and large-scale area averages in the Southwest. The weather systems that bring winter precipitation are large, such that point measurements agree relatively well with large-scale averages (and vice versa); e.g., the correlation coefficient between winter Nogales precipitation and the Climate Division 7 average is 0.94. In contrast, the weather systems that bring summer precipitation are much smaller (or at least the individual storm cells that bring rainfall are much smaller), so that seasonal precipitation averages from individual stations are much less representative of large-scale area averages during summer than during winter (e.g., the correlation between Nogales and Arizona Division 7 precipitation is only 0.53 in summer). Interestingly however, this seasonal difference in statistical character has little effect on the seasonally stratified correlations with the PDO and El Niño (i.e. the correlations for Division 7 show a pattern similar to that shown in Table 1).

Summer trends

The 5 year moving average of the number of peaks for the daily streamflow and the number of daily precipitation occurrences during the summer (July-August) are shown in Figure 2. It can be seen that both records have an apparent decline trend (linear) in the frequency of occurrence. The 5-years moving averages for the total summer precipitation and streamflow are presented in Figure 3. Even though the streamflow values have high variability and few unusual wet summers were observed in the early 50's, a linear regression fitted to the record indicates a downward trend. This linear trend is not apparent in the daily precipitation record. The precipitation record at the Nogales site went through a change in the sampling of the trace amount in the mid 70's, which may be influencing the results shown in Figures 2 and 3. For that reason, the summer precipitation trend requires further analysis.

Similar trends in peak magnitude and number of peak occurrence were documented by Pool and Coes (1999) for the Upper San Pedro Basin in the Charleston gauge. In their analysis, precipitation records from four stations show a slight decline trend in the season totals and a clear indication of summer total flow decrease from 1935 to the 1990's. They further claim that the amount of precipitation that transforms into flow at the channel is also declining for the summer season. Such a trend was not observed for the winter, which favors the assumption that the trend found in summer flow is associated with changing precipitation patterns rather than land use practices and channel improvement. Precipitation changes might be attributed to decreases in storm duration, spatial scale, and/or magnitude of summer precipitation.

A recent study by Thomas and Pool (2006), included a regional statistical survey for Arizona and New Mexico. They found that negative summer trends in streamflow occurred only in the rivers of the Arizona's southwest (i.e., Santa Cruz, San Pedro and Whitewater). This southwestern trend coincides with the seasonal and monthly precipitation trend. However, since precipitation variability is much smaller than the streamflow variability they assumed that there are factors other than precipitation that caused the trend.

In their study Thomas and Cool (2006) evaluated the importance of the following factors as contributors to the trend: increase of temperature which increases evaporation and evapotranspiration; changes in watershed characteristics (upland land cover, riparian vegetation, and the channel morphology); human activity such as groundwater pumping, urbanization, detention structure and cattle ranching; and changes in alluvial storages in the channel banks that releases water into the channel during residing flow. Although, these factors might be interlinked, they assert that natural changes in watershed vegetation cover have the largest effect on the trend. This was based on historical land-cover change evidence in the region, in which upland dessert scrub and grassland vegetation communities have been encroached by Mesquite woodland (Kepner, 1999; Kepner *et al*., 2000). Such changes might have increased summer ET which was found to be a dominant process in streamflow generation in a monthly mass balance study.

Monthly variability

Additional analysis was conducted on the monthly flow values for the Nogales gauge. The monthly flow record which has large variability and is skewed was transformed into a time series with negligible skew and with variance that approaches 1. After experimenting with several transformation methods to yield an approximate normal distribution for the transformed Nogales monthly flow, we used the following transformation steps:

(1) The monthly volumes were transformed using the Box-Cox transformation:

$$x_i = (q_i^{\lambda} - 1)\lambda^{-1} \quad (1)$$

where *i* is index for the month, q is the flow (m^3 $month^{-1}$) and λ is a coefficient that set to 0.1. We experimented with different coefficient values and the selected value appears optimal for reducing the transformed time series coefficient of skewness.

(2) The seasonality in the mean and variance of the transformed flow was removed using:

$$y_{i,j} = \frac{x_{i,j} - \bar{x}_j}{s_j} \quad (2)$$

where *i* and *j* are indices for year and month, respectively, and *x,* $\bar{x}$, and *s* are the flow value, the mean, and the standard variation of the Box-Cox transformed monthly flow.

Figure 4 shows the 24-month moving average of the mean and standard deviation of the transformed and standardized monthly flow. There is no detectable linear trend in the mean while the standard deviation has as apparent positive trend. This trend might be explained as the result of a change in the monthly flow regime that occurred in the mid 1960s. It is apparent that the earlier part of the record has relatively small fluctuations of the mean and standard deviation. Since about 1970, both the mean and the standard deviation time series exhibit larger amplitude fluctuations.

MODELING SCHEME

The modeling of the hydrological system consists of three modules: (1) stochastic generation of the hourly precipitation; (2) transformation of the precipitation into flow at the Nogales gauge site; and (3) simplified ground water recharge for the four microbasins. The development of modules *1* and *2*, parameter estimation and validation are described in detail in Shamir *et al*., (2007), and the interested reader is referred to that reference for more information. In the following sections we only present the salient features of the models for easy reference.

Precipitation Module

An analysis of the precipitation record revealed that during the wet seasons most of the rain events occurred within two hours. This implies that precipitation analysis and modeling should be conducted in fine temporal scale (i.e., hourly). The hourly precipitation module was developed based on analysis of the hourly precipitation record (44 years) from Nogales. The assumption carried in the development of the precipitation module is that the long-term statistics of the point measured precipitation record resemble long term statistics of any given location in the drainage area that is significant for the streamflow generation at the Nogales gauge. The analyzed precipitation gauges which are located in the valley might not represent the orographic precipitation processes that occur on higher elevations. However, it appears that the physical setting of the gauge locations (e.g., elevation, aspect, and land cover) is comparable to most of the basin's drainage area. In addition, as noted above, spatial precipitation simulations from mesoscale atmospheric model showed that, in most cases for winter, the gauge location adequately represented the drainage area (Shamir *et al*., 2007).

The precipitation module is based on a point process model and statistical aggregation of the precipitation events into temporal clusters that represent synoptic weather events. The module characterizes three independent frequency distributions: (1) the inter arrival time of a temporal cluster; (2) the duration of a given cluster; and (3) the

magnitude of an hourly precipitation event. These distributions were approximated by 2-parameter exponential distributions with parameters estimated from the gauge record using the method of moments. To complete the precipitation generation scheme, the distribution of the inter-arrival time of precipitation within the cluster was developed. Such distribution was found to be dependent on the cluster duration, and this dependence is reflected in the model. An important determinant of the precipitation scheme is the identification of clusters, which was accomplished using the statistical procedure of Restrepo-Posada and Eagleson (1982).

Further flow record analysis revealed that the wet seasons (summer and winter) exhibit large inter annual variability. Therefore, an attempt to develop a synthetic module using sample statistics that include all the years from these wet seasons would average very different years and consequently compromise the sampling of the extremes (both dry and wet years). The development of a stochastic module with deterministic trend components that represent the decline in summer flow and the increase in monthly flow variability would yield simulations with extreme (and likely unrealistic) changes when the module is used for simulating long duration time series.

We decided, therefore, to categorize the summer and the winter seasons into wet, medium (normal) and dry years. These categories are based on the observed seasonal flow thresholds. Such categorization implies for both seasons that about 20%, 40% and 40% of the years are wet, medium, and dry, respectively. The selection of these thresholds was subjective and aimed to create three sub-groups that are distinct and with sufficient sample size that would enable reasonable inference from statistical analysis. The module was created for winter and summer and for each season separate modules were created for the three categories (wet, medium and dry). The generation of likely precipitation scenarios for the spring and fall is based on sampling from two independent distributions in each case that characterize hourly precipitation occurrence and magnitude.

Streamflow Module

For the transformation of the hourly precipitation into flow, a conceptual spatially-lumped rainfall-runoff module was developed. This module was implemented

with hourly time steps to simulate hourly flow at the basin outlet. The precipitation rate at the gauge site generates runoff in units of precipitation, which is subsequently converted to mean daily flow for comparison with the observed mean daily flow.

This module implements a calculation of time variant infiltration capacity that depends on the estimated antecedent moisture conditions of the basin. The streamflow from this module is generated as surface flow and interflow. Surface flow results when either the precipitation intensity is higher than the soil infiltration capacity, or the infiltrated precipitation amount produces soil saturation. Interflow generation is dependent on the soil water content and on an interflow constant parameter. For each season, a unique set of the five rainfall-runoff module parameters was identified.

A comprehensive analysis of the performance of this module on daily, seasonal and annual time scales, including its ability to maintain the large variability in the flow is presented in Shamir *et al*., (2007). An example for the module performance is presented in Figure 5. In this Figure the cumulative distribution of the observed daily flow for the four seasons is compared with the daily cumulative distribution from an ensemble of module-simulated daily flow that includes 100 realizations, each of 100 years duration. For winter and summer each realization includes the three precipitation modules of the wetness categories. These categories were applied randomly and independently using the frequencies of the observed streamflow. We used the Box-Cox transformation to transform the highly skewed discharge values into ones that approximately have normal distribution properties. The ranges of variability are large, and this transformation is used to facilitate graphical presentation of the variety of flow magnitudes. The results in the Figure indicate the percent of daily flow events (x-axis) with magnitude that is larger than a given flow value (y-axis). They show that the cumulative distribution of the simulations generally compares well with that of the observations for all four seasons.

Groundwater Module

The Arizona Department of Water Resources (ADWR) has developed a detailed groundwater model that simulates changes in groundwater levels for the southern four microbasins (i.e., Buena Vista, Kino Springs, Highway 82 and Guevavi). The model is

based on the Modular Finite Differences Groundwater Flow Model (MODFLOW) (McDonald and Harbaugh 1988). ADWR conducted a comprehensive validation of the model simulation with historical data for the period of October 1998 – September 2003 with satisfactory results (Erwin, 2007). The execution of the spatially distributed MODFLOW model requires distributed groundwater data and boundary conditions (e.g. streamflow, recharge and evapotranspiration data) and significant CPU time for execution. With the current implementation of this model it is infeasible to run many realizations in ensemble mode to simulate likely groundwater changes over a long period (i.e., 100 years) given a variety of forcings of interest. In order to utilize the simulated surface flow model in ensemble mode, a simplified groundwater model was developed for the 4 microbasins. In formulating the module, the major objective was to develop a simplified module that reliably estimates the simulation of the MODFLOW module for the region of interest.

The module uses a monthly time step and four reservoirs that represent the four microbasins in a spatially-lumped manner. These conceptual reservoirs are assigned effective parameter values and are set in series. For these reservoirs a mass balance equation is posited,

$$S_{i,j} = S_{i-1,j} + I_{i,j} - P_{i,j} - ET_{i,j} \qquad (3)$$

where the subscript i represents the time step, and j is the reservoir number (j = 1,..,4), $S_{i,j}$ is the reservoir content (state of module) j at the end of time step i, I is the infiltration replenishment from the stream into the reservoirs, P is the pumpage withdrawal from the reservoirs, and ET represents losses due to evapotranspiration over the surface area of the microbasins. It is noted that subscript i for fluxes indicates fluxes during time step i.

The infiltration (I) in Equation (3) is estimated as a function of the river flow (Q). It is done by relating the flow discharges to the average wetted width (B) of the stream within the river channel, as follows:

$$B_{i,j} = \alpha_j Ln(Q_{i,j}) + \beta_j \qquad (4)$$

where α and β are estimated coefficients. The potential infiltration capacity into the reservoirs (Ip) is estimated as:

$$Ip_{i,j} = B_{i,j} Kz_j L_j \tag{5}$$

where Kz is the potential infiltration rate, and the L is the channel length in each microbasin. In cases that $Ip_{i,j}$ is smaller than the difference between the capacity ($S_{o,j}$) of the reservoir and the storage of the reservoir after losses have been subtracted ($S_{i-1} - P_i - ET_i$), then,

$$I_{i,j} = Ip_{i,j} \tag{6}$$

otherwise,

$$I_{i,j} = S_{o,j} - S_{i,j} + P_{i,j} + ET_{i,j} \tag{7}$$

The flow at the inlet of the downstream channel that overlays the next reservoir is,

$$Q_{i,j+1} = Q_{i,j} - I_{i,j} \tag{8}$$

The ET flux in Equation 3 is calculated as a function of the Depth to Water (DTW). The DTW was obtained as a linear function of the relative saturation of the reservoirs ($S_{i,j}/S_{o,j}$). The intercept and coefficient of this linear relationship are determined as special cases of the DTW when the relative storage is 0 or 1. The ET is determined as:

$$ET_{i,j} = ETp_{i,j}(1 - DTW_{i,j} / DTW_{o,j}) \tag{9}$$

where the *ETp* represents potential monthly *ET* and DTW_o is the maximum *DTW* for which there is *ET*.

The capacities of the reservoirs ($S_{o,,j}$) are estimated as the maximum storage capacity of the four microbasins [(area)x(basin depth)x(specific yield)]. These values were obtained as averages of the younger alluvium and the combined younger and older alluvium as calculated by the ADWR MODFLOW model for October 2000. During this period, there were about 15 days of flow in the river and the groundwater levels at the microbasins were the highest among those obtained during the simulation period. It is noted that the estimated reservoir capacities are likely to be on the low side as they do not include water that may be extracted by plant roots.

The potential monthly rates of *ET* were obtained from the ADWR model parameterization scheme and are dependent on land cover classifications. For this application the potential rates of *ET* were calculated as a weighted arithmetic mean of the distributed potential *ET* values. These values represent the entire surface area of each microbasin and not only the riparian zones along the alluvial channel. To get the potential *ET* the rate is multiplied by the basin surface area, which was also retrieved from the ADWR model setup.

The development of the linear slope coefficients that relate DTW_j to $S_{,j}$ is based on spatial averages per microbasin of the ADWR MODFLOW simulations. Obvious linear relationships between the average depth to water and the average storages were found ($R^2 > 0.9$), except for the Buena Vista microbasin. For this basin during the simulation period the water level and the storages remain high, which does not provide enough spread to develop a linear regression equation. The regression used for this microbasin utilizes the mean of the other microbasins regression slopes. The DTW_o is estimated as the DTW for which the storage content in the microbasins is 30% of their capacities.

The infiltration coefficients (α and β) were estimated by trial and error for these 5 years using the fluxes from the ADWR-model and the dynamic estimates of infiltration inferred from the observed flow at the Nogales gauge. Note that the wetted width (*B*) is derived in feet and the parameters were estimated with discharge units of cubic feet per month. The *Kz* is set equal to 0.6 meter per day (Erwin 2007). The estimated parameters for the model and other characteristics of the microbasins are provided in Table 2.

The simplified module maintains a very good agreement with the ADWR model for the simulated period (Shamir *et al.,* 2005). In Figure 6 we compare the monthly simulation of *DTW* with index wells in the microbasins. Note that the *DTW* calculated by the module represents an effective groundwater level for the entire surface area of the basin. Therefore, the comparison that is presented here is between areal and point values. In addition, keep in mind that at the monthly time scale shown the data is discrete and it is reasonable to have a non-linear connection between two successive points, so the linear connections shown are only for ease of visual comparison. It can be seen that in most cases the model and the wells follow a similar trend. In all cases but for Buena Vista there is a well that matches model simulations very well. For Buena Vista there is a consistent difference between the DTW of the single available well and the model simulation.

Inter-annual Variability

Up to this point we describe model framework development that concerns the within-year statistical characteristics of precipitation, flow and groundwater levels. The differences from year to year are also important especially in this arid environment that exhibits such extreme differences among the years. In order to represent the year-to-year variability in the long duration simulations (e.g., 100 years) a method to assign a wet, medium or dry category for the summer and winter seasons is needed. In the first ensemble, 100 realizations were created each for 100 years. The year-to-year variability was decided randomly as the chances for the wetness categories were inferred from the observed streamflow record. This ensemble was created such that each year is independently determined by chance. In a second ensemble the interannual variability was determined based on a seasonal reconstructed precipitation estimate derived from a tree ring database that is described in the next section.

Precipitation Time Series Reconstruction from Tree Rings

Annual and seasonal precipitation was reconstructed from a tree ring database. A total of 48 total-width, earlywood-width and latewood-width chronologies between

latitudes 29ºN and 33ºN and longitudes 109ºW and 112 ºW were assembled for the study from the International Tree-Ring Data Bank (http://www.ncdc.noaa.gov/paleo/treering.html) and computer files of the Laboratory of Tree-Ring Research at the University of Arizona. The tree ring chronologies were screened against Nogales seasonal precipitation, 1914-2000, by linear regression and sets of chronologies with a statistically significant seasonal precipitation signal were applied to reconstruct precipitation using a regression modeling approach described in Meko (1997). A detailed description of the precipitation reconstruction procedure is provided in Shamir *et al*. (2005 Appendix A).

The strongest tree-ring signal for precipitation was found for the winter season. The reconstruction that is based on two principal components of 24 screened chronologies for winter yielded a reconstruction covering the period 1647-1966. This reconstruction explained 57% of the variance of observed winter precipitation in the 1914-66 calibration period and exhibited positive skill of cross-validation, with a reduction of error statistic (Fritts *et al*. 1990) of 0.50.

The winter reconstruction was the only seasonal reconstruction used in this study as reconstructions for other seasons, while statistically significant, explained much smaller percentages of observed precipitation variance. In Figure 7 the annual time series of winter precipitation and the time series smoothed by various 10 and 25 years moving average, are presented. It can be seen that the 10-year smoothing retains considerable variability, with lows near 1670, 1820, 1890 and 1955, and largest positive departure early in the 20th century.

Three existing tree-ring reconstructions of climate variables more-or-less relevant to the southern Arizona region were examined to check the consistency of low-frequency fluctuations with those in reconstructed Nogales winter precipitation. The first comparison series is from a network of reconstructions of summer-average Palmer Drought Severity Index (PDSI) on a 2.5 x 2.5 degree grid over much of North America (Cook *et al.,* 2004). The series used are for the gridpoint nearest Nogales (32.5N, 110W). The second series is a reconstruction of cool-season (November-April) precipitation for the San Pedro Basin, Arizona, from total-width tree-ring indices (Meko, 1997). The third series is a reconstruction of cool-season (November-April) precipitation for Arizona

Climate Division 7 from Ni *et al. (*2002). This last series is a reconstruction of divisional-average precipitation from a network of specially screened 1000-year long tree-ring chronologies, mostly from the Four Corners area.

In Figure 8 the low-frequency components of reconstructed winter and the three other reconstructed time series are compared. The series are presented as Z-scores, which indicate the distance and direction of the variables from the sample mean in order to eliminate differences caused by the scale of the individual variables. Reconstructed winter precipitation appears most closely to track the reconstructed PDSI series, with major lows coinciding near 1670, 1730, 1820, 1890 and 1950. Least similar is the reconstructed Division 7 precipitation, which has several major features not shared with winter (e.g., the drought near 1770). The discrepancies with the Division 7 reconstruction can be explained by the remote location of the tree-ring sites from Nogales.

The reconstructed precipitation which is valid only for the winter season is used to determine the winter categories of Wet, Medium, or Dry for the second ensemble. Using such approach carries an assumption that the intra-annual precipitation distribution in the paleoclimatic record is the same as in the historical record. In other words, a wet/dry year in the 20th century has the same statistical characteristics as a wet/dry year in the 18th century. Since these winter categories were determined based on the annual yield of flow (not precipitation), a statistical relationship between the annual precipitation and annual flow was established. The winter record of the tree-ring reconstructed precipitation was divided into quartiles and for each quartile the frequency of occurrence of a wet, medium or dry winter flow season was determined. These frequencies of occurrence for the different winter categories are presented in Table 3. It can be seen that there are clear relationships between the categories and the total precipitation from the reconstructed record. For example, the wet winter flow category occurs only when the precipitation is in the fourth (highest) quartile and the dry winter flow category does not occur when the precipitation is in the fourth quartile. Moreover, the chance for a dry winter flow category to occur decreases with increasing precipitation quartiles. The dominant flow regime is in the Medium winter flow category and occurs at about 57% of the years followed by the dry (27%) and the wet (16%) winter flow categories.

One hundred realizations of the module each for 319 years (length of tree ring reconstructed precipitation record) were generated. For each year the selection of the winter categories was made by Monte-Carlo sampling that used the frequencies of Table 3. Examples of generated winter flow (total season) are shown in Figure 9. The flow values in this Figure were transformed using the Box-Cox transformation for clarity. The plots show that there are long (even centennial) periods with relatively low flow variability followed by frequent high flow years. A good example is in the upper panel in which the first 50 years show low flows with very low variability while even the first 100 years only show about 4 periods of higher flows. After the first hundred years, the flow variability increases significantly with frequent periods of high flows to decrease again near the end of this generated record. This type of behavior suggests caution when inferences are derived from the historical gauge record only (record lengths of less than 100 years).

The effect of the long term memory of the flow Wet, Medium and Dry categories is exemplified in Figure 10. In this Figure the cumulative departure of each realization from the realization mean annual total flow (upper panel) and winter flow (lower panel) are plotted. The 5, 50 and 95 percentiles are marked in black. A negative gradient in this Figure means that the deficit from a given reference point is increasing while a positive gradient indicates that the surplus relative to the reference point is increasing. Visual inspection indicates that in general the negative gradient of the median has longer stretches than the positive gradient. This indicates that the periods of stress (droughts) and deviation from the base reference are longer than the wetter periods.

It is noted that the relationships between the PDO and El Nino – Southern Oscillation (ENSO) climatic indices and the winter flow categories were found weaker than those found for the tree-ring reconstructed precipitation, and were not used in the simulations.

RISK ASSESSMENT

In this section we exemplify the utilization of the aforementioned modeling framework for watershed management and long term planning. The simplified groundwater module for the microbasins was forced by a 100 realizations ensemble of

the monthly aggregate, each of 100 years length, to produce an ensemble of groundwater storages and levels in the four microbasins. Different annual pumping rates from the microbasins were assigned as a percentage of the microbasins capacities. The ranges of the pumping withdrawals are from no pumping to pumping at 50% of the microbasin capacity. The annual pumping withdrawals were distributed equally among the months. In each ensemble, the conceptual groundwater reservoir initial storage condition was assigned randomly from a uniform distribution using the range of possible reservoir storages. The first year of simulations was discarded for the analysis to follow.

Figure 11 shows the fraction of time with groundwater reservoir storage below an indicated threshold as a function of the pumping rate. The thresholds in this case were defined as 25% 50% and 75% (upper, middle and lower panels, respectively) of the microbasin reservoir capacity. Many of the reservoir response characteristics can be discerned from this figure. It can be seen for example, that the Buena Vista and Guevavi are more sensitive reservoirs and for large pumpage values the storage of these reservoirs is below the thresholds most of the time. However these two reservoirs are different one from the other in their response and sensitivity to increasing withdrawals. The Buena Vista microbasin has a small pumpage range tolerance for different thresholds, in that the reservoir storage moves sharply from being above the threshold to being below it most of the time. The Guevavi microbasin shows a more gradual change in going below the storage threshold with increasing withdrawals. The Kino Springs and Highway 82 microbasins also show a gradual increase in the frequency of going below the thresholds with increasing withdrawals, although, much smaller than that of Guevavi. No apparent differences were observed between the results of Figure 11 and those created using the above described analysis for an ensemble that includes 1000 realizations.

In Figure 12 and for various pumping scenarios we explore the uncertainty in groundwater content that is associated with the variability of the streamflow predictions. In this Figure, the median, 5, and 95 percentiles of the 100 realizations are shown, but this time only for the 50% reservoir storage threshold. The uncertainty in this Figure is fairly constant and can be estimated at about ±10%. It implies that by representing the variability in the observed precipitation and streamflow as discerned from the gauge record, the uncertainty in predicting the fraction of the time that the microbasins

reservoirs will be below 50% of their storage capacity is within 10%. This uncertainty bound is established for a 100-year simulation. Again no apparent differences were observed in the uncertainty bound for an ensemble that has 1000 realizations.

An additional management and planning concern is the duration of the potential reservoir stress. In other words, a persistent stress of the aquifer might be a larger concern than occasional stresses. In Figure 13, we analyze a single realization of 100 years for the number of occurrences for which the microbasins have shown consecutive monthly stresses. These stresses are ranged from 1 to 20 consecutive months (x-axis). The stress in this example is defined as reservoir storage being below 50% of its capacity. These consecutive stress periods were exploited with different levels of pumping rates. The Figure again presents the difference in the response of the four microbasins to different rates of withdrawals. The Buena Vista and Guevavi reservoirs have a critical pumping value that, if exceeded, puts the reservoirs in persistent stress. The other two reservoirs are more sensitive to the climate variability and can recover more easily after a stress period. In Figure 14 the same analysis is repeated for an ensemble with 1000 realizations. We note that the occurrence of the consecutive stresses in all microbasins appear more frequent in the 1000 members ensemble.

In Figure 15 the ensemble is analyzed to provide uncertainty bounds for the consecutive occurrence of stressed microbasins (storage less than 50% of the capacity) for a pumpage scheme of 40% of the capacity. This estimate of uncertainty is a result of precipitation variability. It can be seen that the microbasins show a range of different uncertainty bounds. In general it can be said that compared with Kino Spring and Hy 82 microbasins, the Buena Vista and Guevavi microbasins have higher probability for consecutive monthly stress that is associated with wider uncertainty bounds.

The above analysis was also conducted with the ensemble of streamflow that is based on the paleoclimatic precipitation estimates from tree-ring records. This ensemble has a record duration of 319 years. The results of the stress frequency of occurrence appear very similar to the analysis presented above when the entire paleoclimatic record was analyzed. In a second experiment with results shown in Figure 16, the entire ensemble record of 319 years was divided into 14 different ensembles; each ensemble of a 100 consecutive years duration that span the entire paleoclimatic record with 200-

month intervals. The spread among the realizations in the Figure represents the uncertainty that is associated with both within-year and year-to-year variability in different 100-year sections, as discerned from the paleoclimatic precipitation estimates. Comparing Figures 12 and 16 makes the difference in uncertainty in the groundwater content results apparent for the two cases: *(a)* when only the historical record is used, and *(b)* when the paleo-climatic record is used. The breadth of the 5-95 percentile bands around the median is significantly higher when paleoclimatic information is used for all cases. Suggesting that because of the significant additional long-term variability, the historical record cannot in itself lead to reliable risk definitions.

In the simplest utilization of this model as a planning tool, the user can define deterministic thresholds that signify the aquifer stress and the acceptable risk to have stressed aquifer. Assignment of these variables is not a trivial task. For example the definition of stressed aquifer can be looked from a variety of perspectives such as for example: support of riparian ecology, risk of land fissures and subsidence; the economic value of water exploration; and water quality standards. Each of these listed objectives is likely to yield a different definition of stress.

SUMMARY AND CONCLUSIONS

A model framework for long term planning of water resources in the upper Santa Cruz River, Southern Arizona is presented. This framework consists of three hydrologic modules: 1) a point process stochastic module of hourly precipitation scenarios that maintains the characteristics and variability of a 45-year hourly precipitation record from nearby rain gauges; 2) a conceptual module that transforms the precipitation into streamflow using varied infiltration rates and estimates the basin's antecedence moisture conditions; and 3) a simplified groundwater module for four downstream microbasins that accounts for alluvial groundwater recharge, and ET and pumping losses.

Long term (i.e., 100 years) realizations (forming an ensemble) are generated by the above described model framework for two different regimes of inter annual variability. The first regime is that of the historical streamflow record and the second regime is based on reconstructed paleoclimatic precipitation estimates. For the latter,

winter-season and annual precipitation were reconstructed for the Nogales gauge site based on tree ring chronologies.

A risk assessment case study was conducted in which the two flow ensembles (historical and paleoclimatic) were used to evaluate the risk of each of the four microbasins declining below a predefined groundwater content threshold. Risk was measured in terms of the frequency of both a single and several consecutive occurrences of aquifer storage declines below a selected threshold.

Perhaps the main conclusion of this work is that this modeling framework may be used to produce likely future scenarios of streamflow for screening risk analyses pertaining to the likely behavior of the groundwater volume and level in the microbasins of the south Santa Cruz River region under a variety of development scenarios. The simulations and results obtained indicate that preserving both within-year and year-to-year variability is necessary to approximate the total uncertainty in future flow simulations. The results also show that the risk associated with a microbasin being in a stress state is different for each microbasin and depends significantly on the physical properties, pumping rates, and the sampling uncertainty in the forcing streamflow ensemble, especially for consecutive stress periods. The risk response is also found to be non linear with respect to pumping and stress storage threshold.

Main recommendations for future studies are *(a)* the use of risk analysis as exemplified in this work in collaboration with regional officials and agencies to establish policy regarding regional development in the microbasins region of the south Santa Cruz River; *(b)* assessment of this modeling framework in other semi-arid or arid regions; and *(c)* incorporation of climate change scenarios to possibly improve the generation of future ensembles of streamflow.

Acknowledgments. Support for this work was provided by Arizona Department of water Resources (ADWR) Santa Cruz Active Management Area under contract # 2005-2568. Special thanks are extended to the ADWR personnel Frank Corkhill, Gretchen Erwin, Keith Nelson, Frank Putman, and Alejandro Barcenas for providing data and information and for their useful comments on the risk-based approach followed. We would like also to thank three anonymous reviewers for their constructive criticism. The opinions expressed herein are those of the writers and do not necessarily reflect those of the funding agency.

LITERATURE CITED

Alley, W. M., 2001. Ground Water and Climate. Ground Water (39):2-161.

Arizona Department of Water Resources (AZDWR) December 1999. Third Management Plan for the Santa Cruz Active Management Area 2000-2010.

Cayan, D. R., M. D. Dettinger, H. F. Diaz, and N. E. Graham, 1998. Decadal Variability of Precipitation over Western North America. Journal of Climate 11:3148-3166.

Cook, E. R., C. Woodhouse, C. M. Eakin, D. M. Meko, and D. W. Stahle, 2004. Long-Term Aridity Changes in the Western United States. Science 306:1015-1018.

Erwin, G., 2007. Groundwater flow model of the Santa Cruz Active Management Area microbasins international boundary to Nogales international wastewater treatment plant Santa Cruz County, Arizona, Arizona Department of Water Resources, Modeling report #15

Fritts, H. C., J. Guiot, and G. A. Gordon, 1990. Verification. In Methods of Dendrochronology, Applications in the Environmental Sciences (ed E. R. Cook and L. A. Kairiukstis), Kluwer Academic Publishers, p. 178-185

Gleick, P. H., and D. B. Adams, 2000. Water the Potential Consequences of Climate Variability and Change of Water Resources of the United States: The Report of the Water Sector Team of the National Assessment of the Potential Consequences of Climate Variability and Change for the U.S. Global Research Program, 151 Pp Pacific Institute for Study in Dev Environment and Security, Oakland CA .

Halpenny, L.C., and P. C. Halpenny, 1991. Renewable Urban Water Supplies, Nogales and the Microbasins of the Santa Cruz River, A Case of Natural Water Banking:

Fifth Biennial Symposium on Artificial Recharge on Groundwater: Challenges of the 1990s, Tucson, Arizona.

Hanson, R. T. and M. D. Dettinger, 2005. Ground Water/Surface Water Responses to Global Climate Simulations, Santa Clara-Calleguas Basin Ventura, California. Journal of the American Water Resources Association (June 2005):517-536.

Kaplan, A., M. A. Cane, Y. Kushnir, B. Blumenthal, and B. Rajagopalan, 1997. Analysis of Global Sea Surface Temperature 1856-1991. Journal of Geophysical Research 101: 22599-22617.

Kepner, W. G., C. J. Watts, C. M. Edmonds, J. K. Maingi, S. E. Marsh, G. Luna, 2000. A Landscape Approach for Detecting and Evaluating Change in a Semi-arid Environment. Journal of Environmental Monitoring and Assessment 64 (1):179-195.

Kepner B, 1999. San Pedro River – A landscape approach to community based environmental protection: U.S EPA fact sheet.

Mantua, J. N., S. R. Hare, Y. Zhang, J. M. Wallace, and R. C. Francis, 1997. A Pacific Interdecadal Oscillation with Impacts on Salmon Production, Bulletin of American Meteorology Society 78:1069-1080.

McDonald M. G., and A. W. Harbaugh, 1988. A Modular Three Dimensional Finite-Difference Ground-water Flow Model, U.S. Geological . Survey. Technical Water Resources Investment. Book 6, Chap. A1.

Meko, D.M. 1997. Dendroclimatic Reconstruction with Time Varying Subsets of Tree Indices. Journal of Climate 10:687-696.

Meko D. M. and C. H. Baisan, 2001. Pilot Study of Latewood-Width of Confers as an Indicator of Variability of Summer Rainfall in the North American Monsoon Region. International Journal of Climatology 21:697-708.

Ni F., T. Cavazos, M. K. Hughes, A. C. Comrie. and G. Funkhouser, 2002. Cool-Season Precipitation in the Southwestern USA Since A.D. 1000: Comparison of Linear and Nonlinear Techniques for Reconstruction. International Journal of Climatology 22:1645-1662.

Pool, D. R and A. L. Coes, 1999. Hydrogeologic Investigation of the Sierra Vista Subwatershed of the Upper San Pedro Basin, Cochise County, Southeast Arizona. *USGS* Water-Resources Investigation Report 99-4197. United States Geological Survey, Tucson Arizona.

Pool, D.R., 2005, Variations in Climate and Natural Recharge in Southeast Arizona: Water Resources. Research 41, W11403, doi:10.1029/2004WR003255, 24p.

Redmond, K. T. and R. W. Koch, 1991. Surface Climate and Streamflow Variability in the Western United States and their Relation to Large-Scale Circulation Indices. Water Resources Research 27:2381-2399.

Restrepo-Posada, P. J., and P. S. Eagleson, 1982. Identification of Independent Rainstorms. Journal of Hydrology 55:303-319.

Shamir E., N. E. Graham, J. Wang, D. M. Meko, and K. P. Georgakakos, 2005. Stochastic streamflow scenarios for the Santa-Cruz River at the Nogales gauge, Prepared for the Arizona Department of Water Resources, Santa Cruz, AMA, Hydrologic Research Center Technical Report No. 4.

url:http://www.hrc-lab.org/projects/dsp_projectSubPage.php?subpage=santacruz

Shamir E., J. Wang, N.E. Graham, K. P. Georgakakos, 2007. Stochastic Streamflow Generation Model for Data Sparse Arid Watersheds. Journal of American Water Resources Associations (accepted)

Sheppard, P. R., A. C. Comrie, G. D. Peckin, K. Angersbach, and M. K. Hughs, 1999. The Climate of the Southwest. Tucson AZ Institute of the Study of Planet Earth, University of Arizona 39 pp.

Thomas, B., and D. R. Pool, 2006. Seasonal Precipitation and Streamflow Trends in Southeastern Arizona and Southwestern New Mexico: U.S. Geological Survey Professional Paper 2005-1712, 79 p.

Webb, R., and J. L. Betancourt, 1990. Climatic Variability and Flood Frequency of the Santa Cruz River, Pima County, Arizona. USGS Open –File Report 90-553. United States Geological Survey, Reston, Virginia.

World Commission on Environment and Development, 1987. Out Common Future. London: Oxford University Press.

Zhang. Y., J. M. Wallace, and D. S. Battisti, 1997. ENSO-like Interdecadal Variability: 1900-93. Journal of Climate 19:1004-1020.

Tables

Table 1. Correlation Coefficients of Climatic Indices with the Nogales Seasonal Precipitation Record, 1914-2000.

	NINO3	PDO	ARIZ. DIV. 7
Winter	0.53	0.27	0.94
Spring	0.11	0.22	0.70
Summer	-0.06	0.09	0.53
Fall	-0.03	-0.09	0.87

Table 2. Microbasin Characteristics and Parameters

	Buena Vista	Kino Springs	Hy 82	Guevavi
Basin area (km^2)	4.7	3.4	6.4	6.0
Basin storage (10^6 m^3)	3.4	5.0	7.3	9.8
Channel length (km)	4.1	6.2	8.0	4.6
		Infiltration parameters		
α	0.5	1.4	3.7	3.45
β	-0.57	-7.6	-3.35	-4.3
		Storage to DTW		
Slope (m / storage fraction)	-17.9	-22.3	-13.8	-17.6
		Potential ET (meter per month)		
April	0.003	0.0002	0.0003	0.005
May	0.025	0.002	0.0024	0.036
June	0.054	0.045	0.045	0.072
July	0.051	0.042	0.045	0.072
August	0.045	0.036	0.042	0.063
September	0.026	0.0021	0.0024	0.063
October	0.006	0.0048	0.006	0.009
November	0.0006	0.0045	0.0006	0.0009

Table 3. The Frequency of Occurrence of Tree-Ring Reconstructed Precipitation Quartiles that Correspond to Winter Flow Categories.

Winter flow categories	Precipitation quartiles from tree-ring record			
	1st	2nd	3rd	4th
Wet	0	0	0	0.625
Medium	0.5	0.69	0.75	0.375
Dry	0.5	0.31	0.25	0

Figures

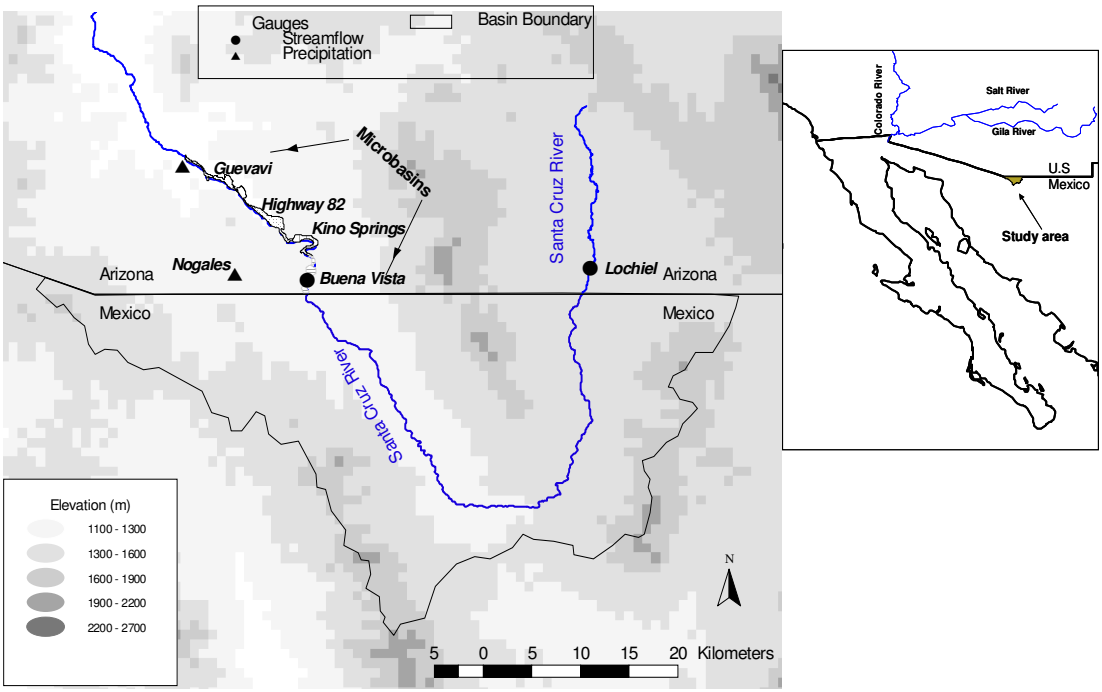

Figure 1. Map of the Region

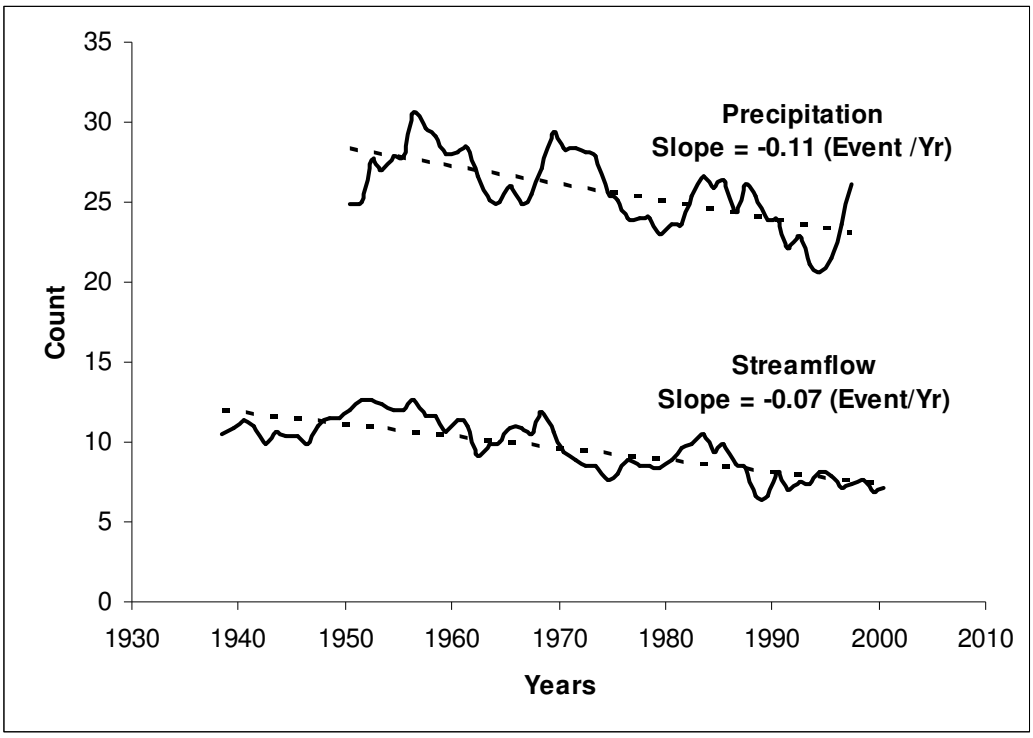

Figure 2. The Nogales summer (July-August) 5-year moving average of the number of streamflow peaks and the daily precipitation events. The slopes of a linear regression fit are also indicated in each case**.**

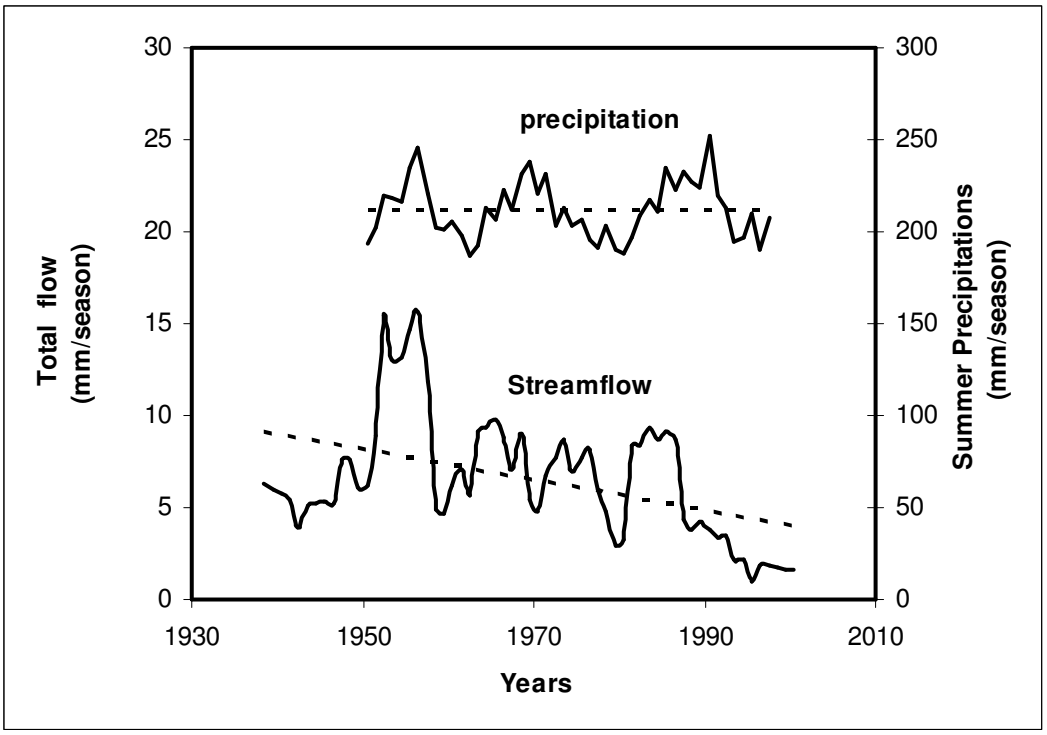

Figure 3. The Nogales summer (July-August) 5-year moving average of cumulative flow normalized for the drainage area (left y-axis) and analogous results for the seasonal cumulative precipitation (right y-axis) are shown. Linear regression fits are plotted for each case.

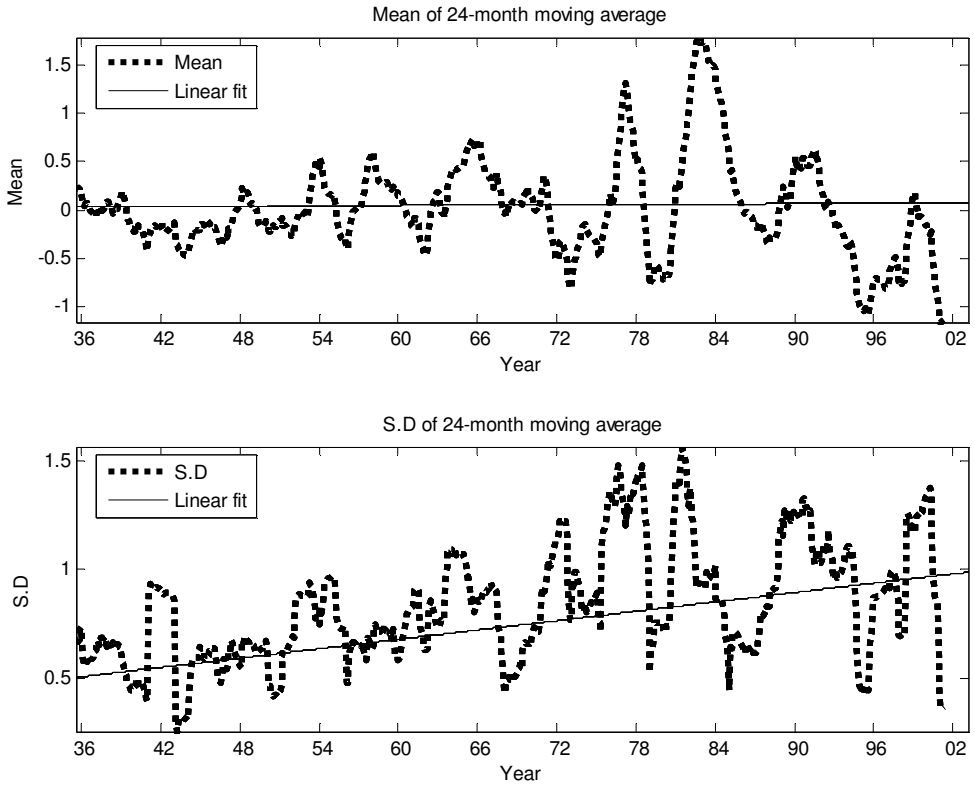

Figure 4. Moving average of 24-month duration for the mean and standard deviation of the observed transformed and standardized monthly flow time series.

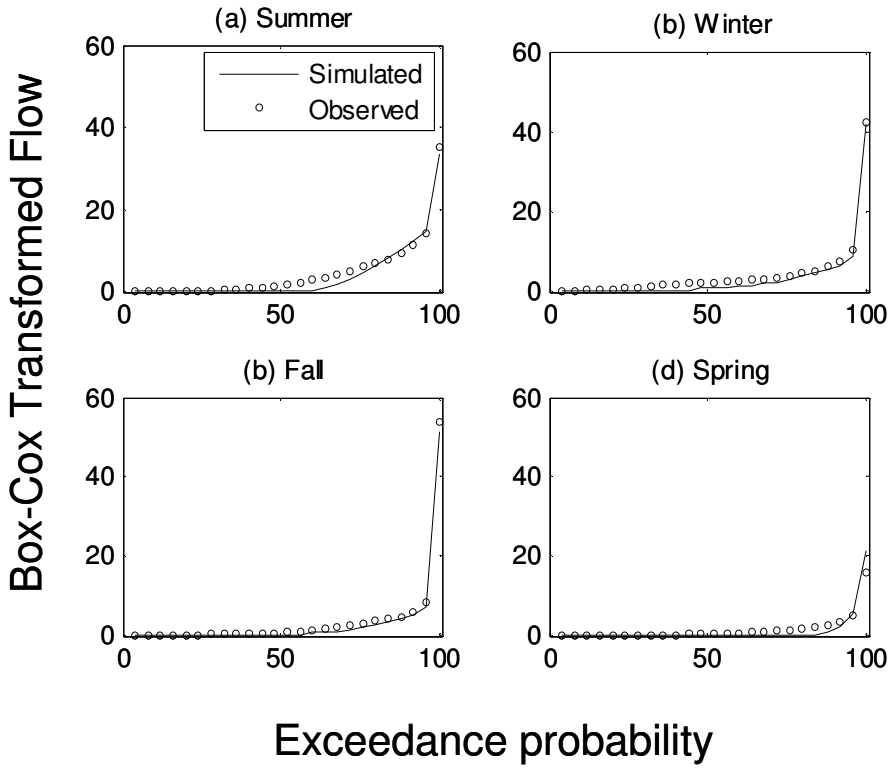

Figure 5. Exceedance plots of the daily Box-Cox transformed flow of 68 years of observation (black circles), and 100 realizations of generated flow, each with a duration of 100 years of synthetic flow (black line).

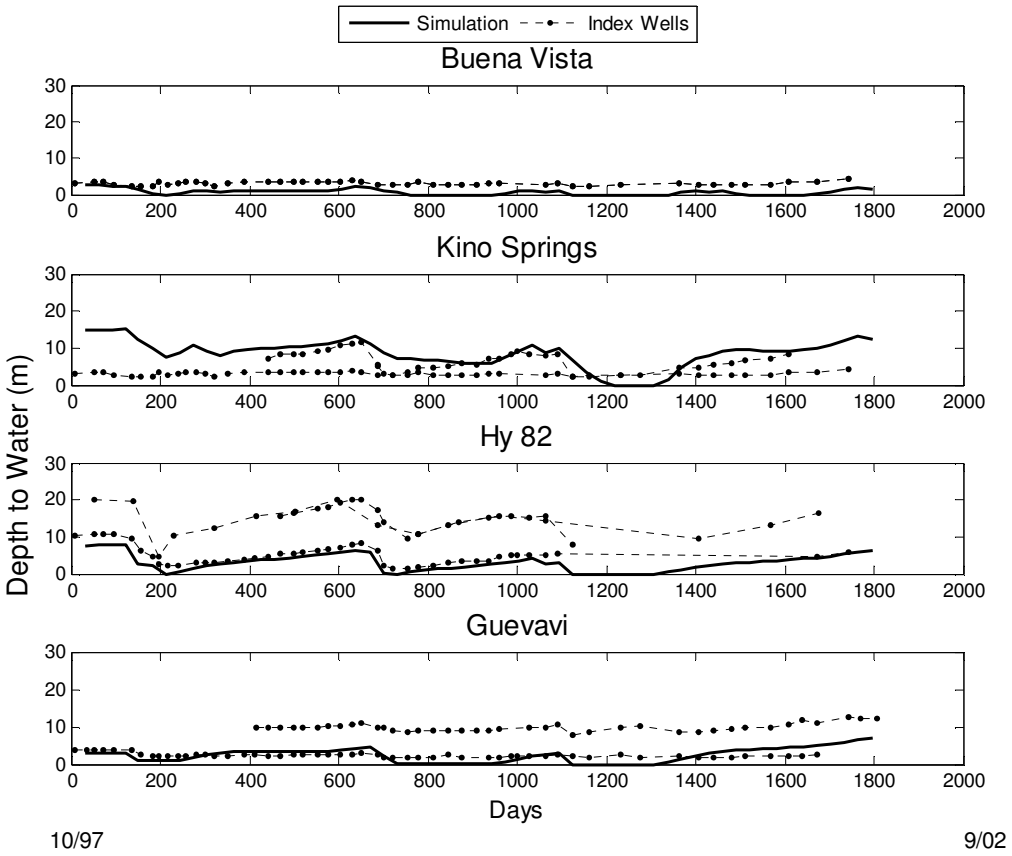

Figure 6. Depth to water comparison between monthly simulations and index wells observations in the corresponding microbasins.

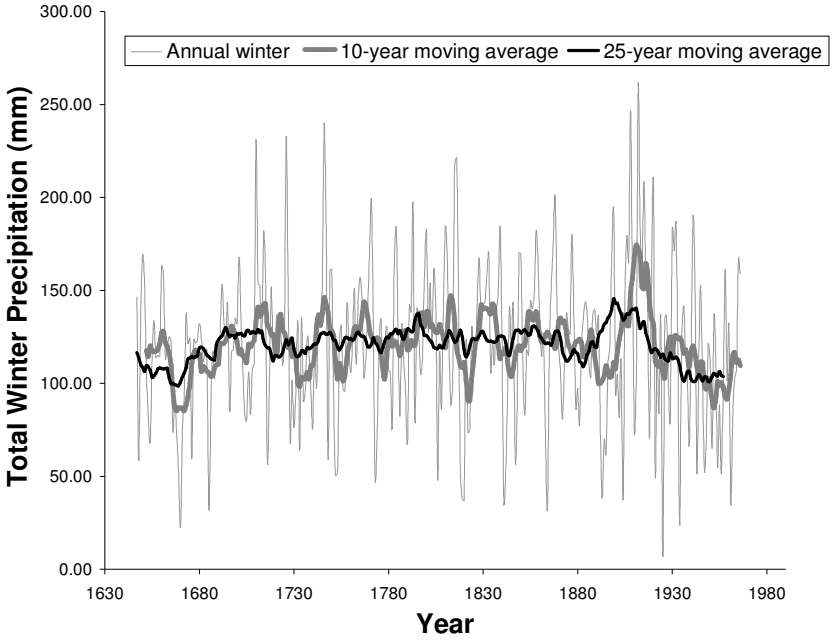

Figure 7. Unsmoothed annual, and 10 and 25 years moving average of the long-term reconstructed total winter precipitation from tree ring chronologies for Nogales.

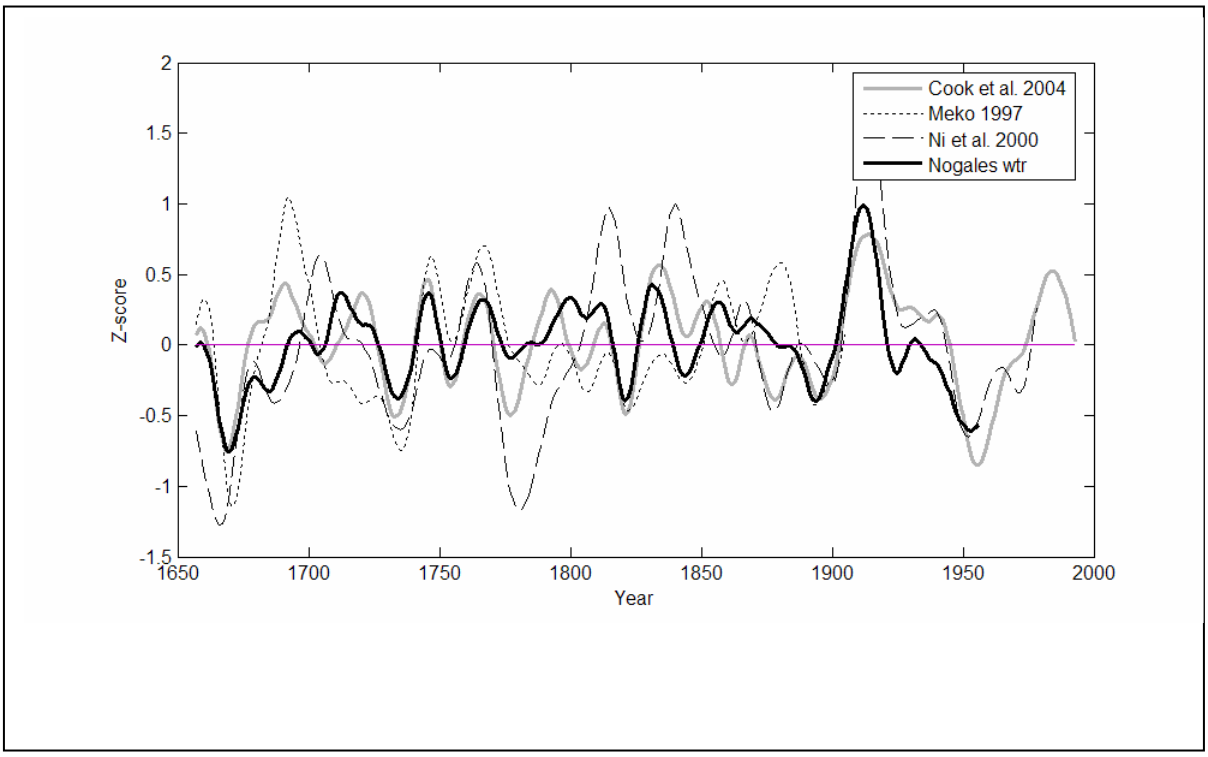

Figure 8. Comparison of smoothed (25 –year Gaussian smoothing) time series of Nogales reconstructed winter precipitation and other relevant paleoclimatic reconstructions.

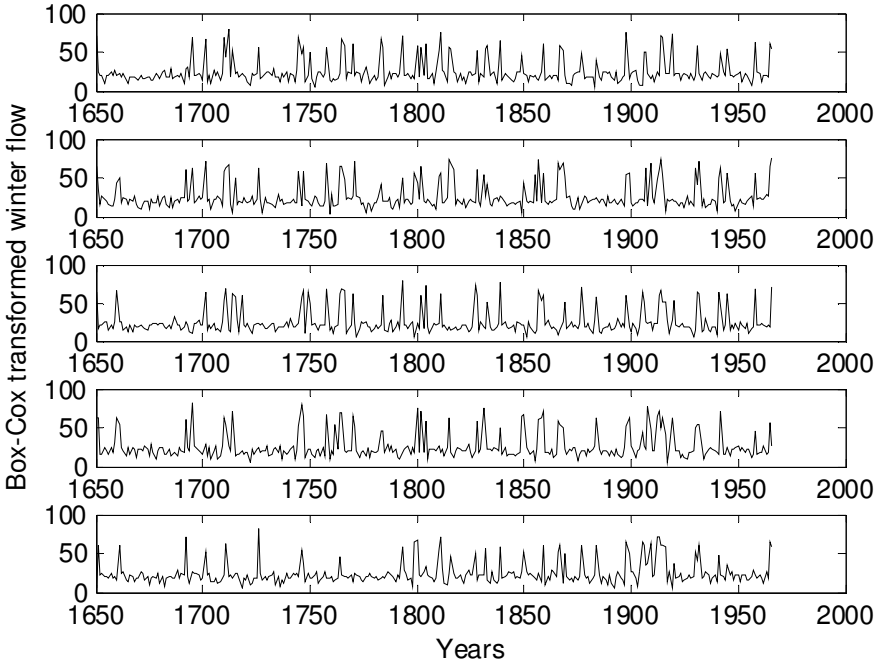

Figure 9. Five model realizations of winter total streamflow for the duration of the tree ring record.

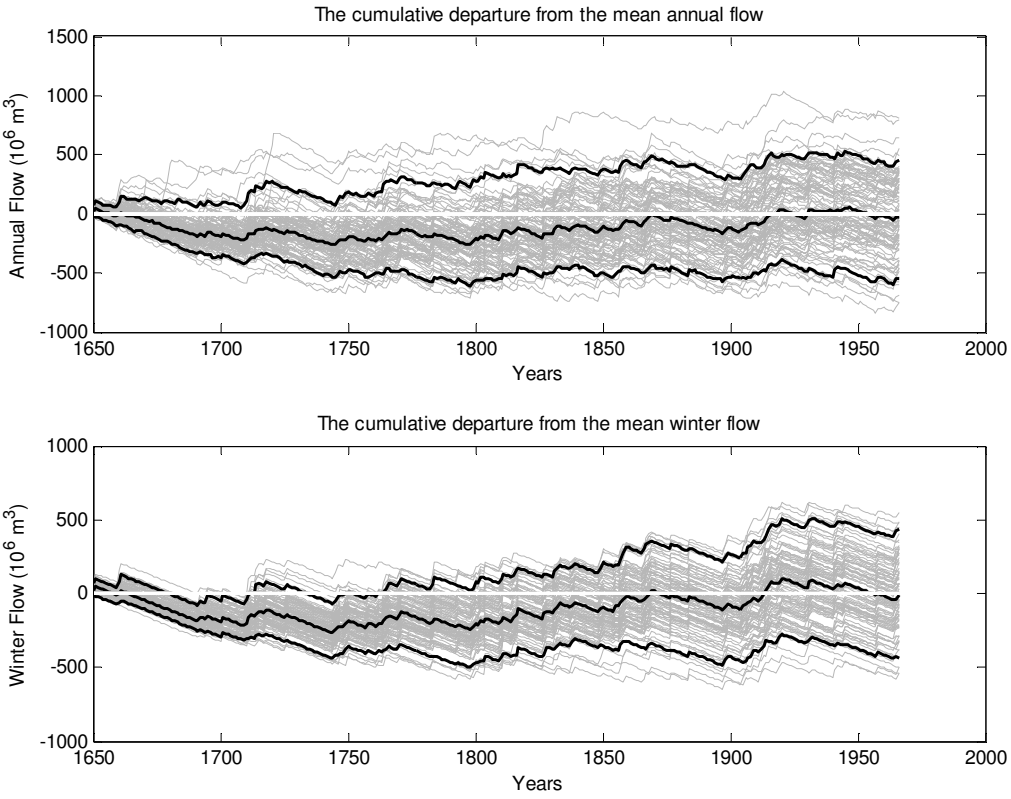

Figure 10. Ensemble of 100 cumulative flow departures from the annual (upper panel) and winter (lower panel) flow means. The ensemble flows maintain the year-to-year variability in the dendrochronology reconstructed precipitation record. Black lines are for the 5, 50 and 95 percentiles of the ensemble.

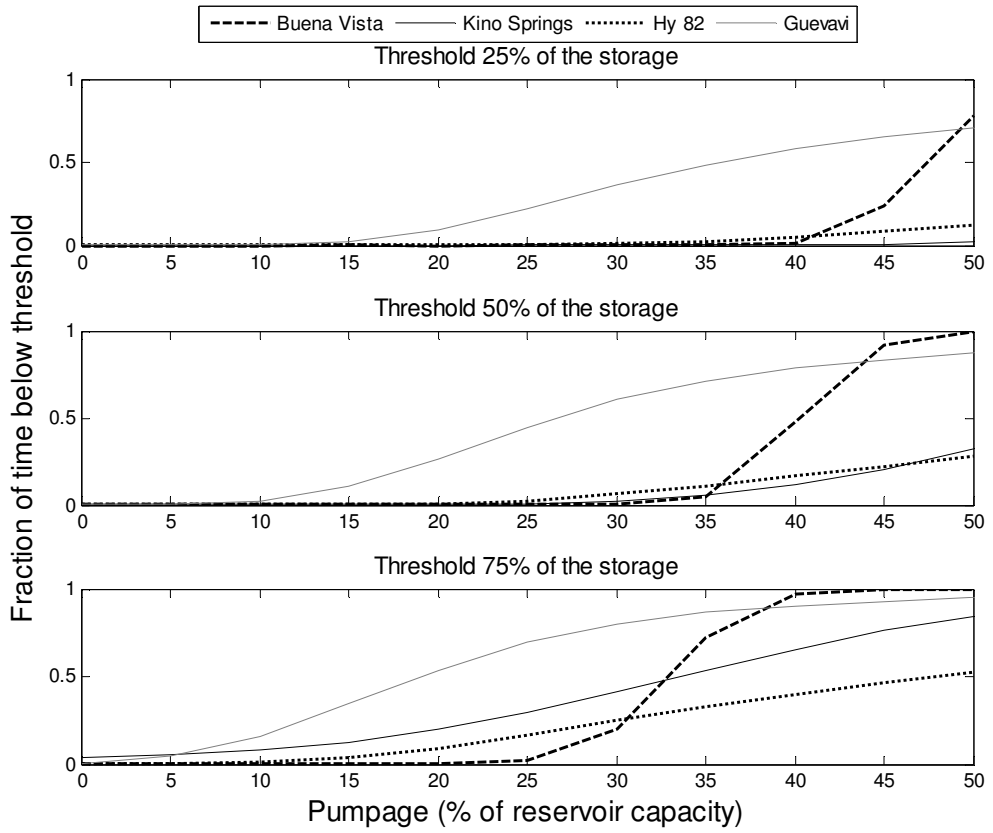

Figure 11. The fraction of the time during 100 years that the monthly water storage in the microbasins is bellow 25, 50 and 75% (upper, middle and lower panels, respectively) of capacity, as a function of the annual pumpage from the reservoirs. A total of 100 realizations of storage sequences are used.

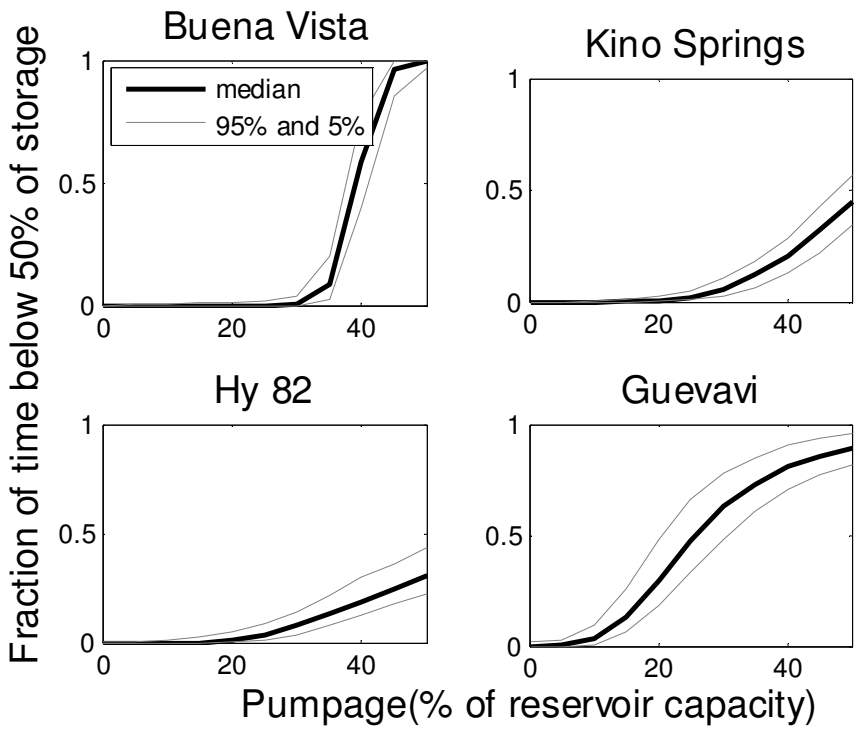

Figure 12. The fraction of the time during 100 years that the monthly water storage in the microbasins is below 50% as a function of the annual pumpage from the reservoirs. The black solid line is the median and the gray lines are the 5 and 95 percentiles as determined from 100 realizations.

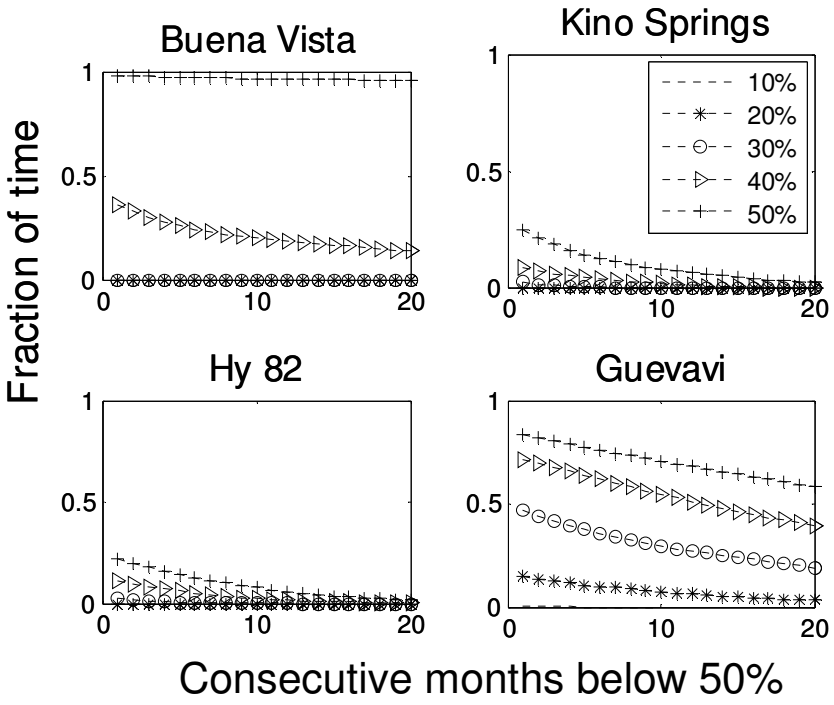

Figure 13 The number of consecutive months with microbasin storage below 50% of capacity determined from a single realization of 100 years. The different lines represent different pumpage schemes.

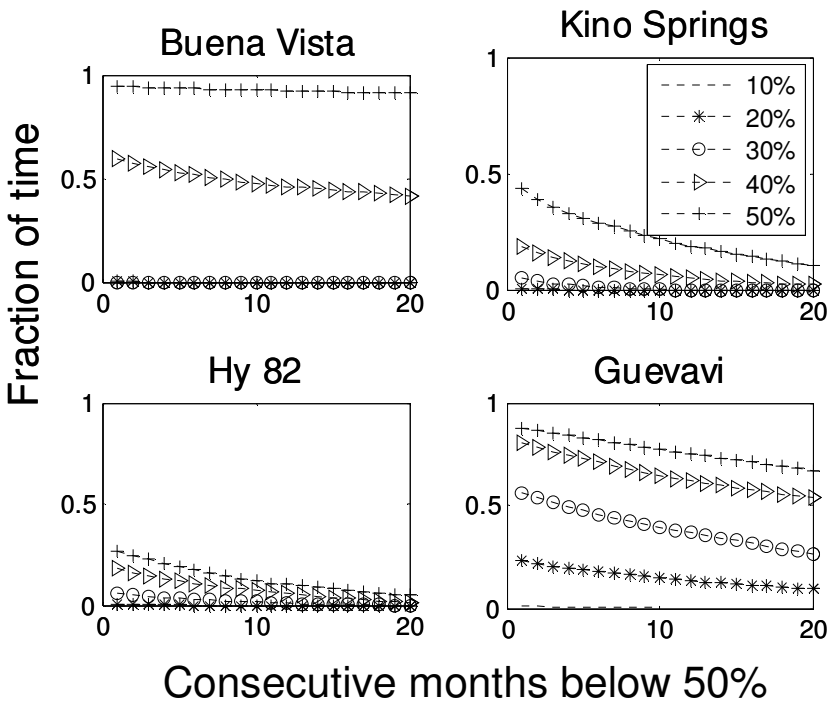

Figure 14. As in Figure 13, but created from an ensemble that has 1000 realizations, 100-years long each.

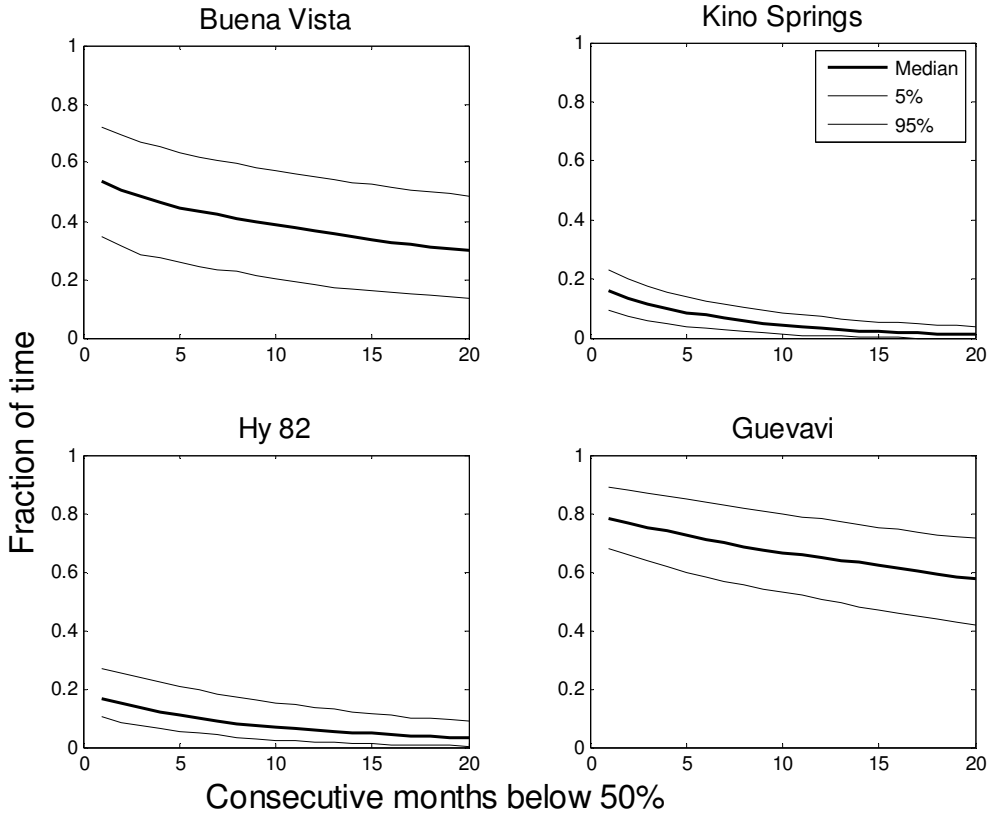

Figure 15. Median, 5 and 95 percentiles of the number of consecutive months with microbasin storage that is below 50% of capacity as determined from a 100 realizations of 100 years each, and for annual pumpage that is 40% of the microbasin capacity.

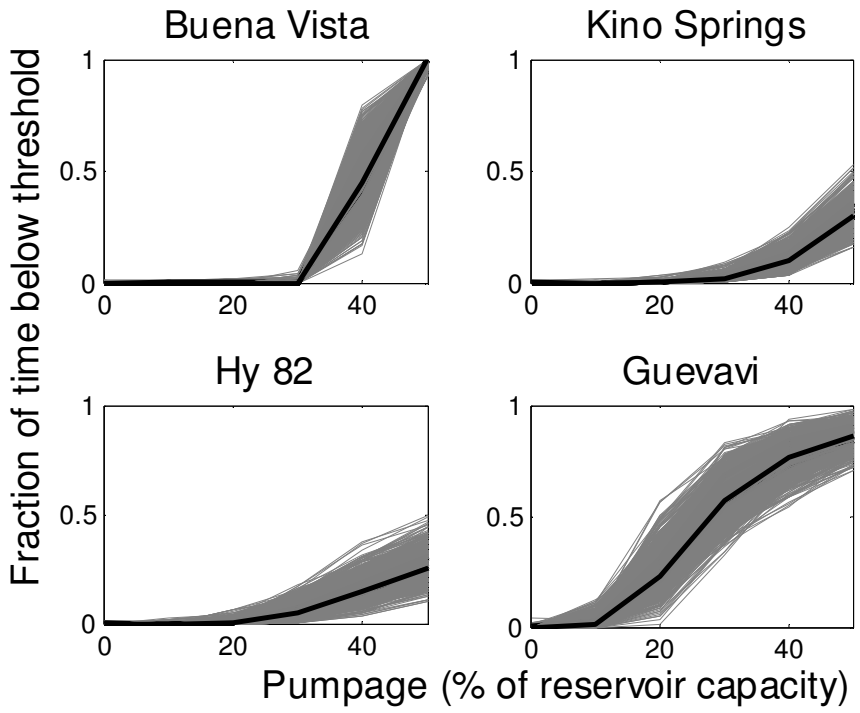

Figure 16. The fraction of the time during 100 years that the monthly water storages in the reservoirs are below 50% of capacity as a function of the annual pumpage from the reservoirs. The gray lines represent the ensemble members derived from 14 ensembles that represent the long-term variability that corresponds to the paleo-climatic record. Each of the 14 ensembles is 100 years long. These ensembles start in 200-month intervals and span the paleo-climatic record of 319 years.